

ARTICLE OPEN



Unprecedented 21st century heat across the Pacific Northwest of North America

Karen J. Heeter¹✉, Grant L. Harley², John T. Abatzoglou³, Kevin J. Anchukaitis⁴, Edward R. Cook¹, Bethany L. Coulthard⁵, Laura A. Dye⁵ and Inga K. Homfeld⁶

Extreme summer temperatures are increasingly common across the Northern Hemisphere and inflict severe socioeconomic and biological consequences. In summer 2021, the Pacific Northwest region of North America (PNW) experienced a 2-week-long extreme heatwave, which contributed to record-breaking summer temperatures. Here, we use tree-ring records to show that summer temperatures in 2021, as well as the rate of summertime warming during the last several decades, are unprecedented within the context of the last millennium for the PNW. In the absence of committed efforts to curtail anthropogenic emissions below intermediate levels (SSP2–4.5), climate model projections indicate a rapidly increasing risk of the PNW regularly experiencing 2021-like extreme summer temperatures, with a 50% chance of yearly occurrence by 2050. The 2021 summer temperatures experienced across the PNW provide a benchmark and impetus for communities in historically temperate climates to account for extreme heat-related impacts in climate change adaptation strategies.

npj Climate and Atmospheric Science (2023)6:5; <https://doi.org/10.1038/s41612-023-00340-3>

INTRODUCTION

Surface air temperatures and the frequency and intensity of extreme heat events are increasing globally and are consequences of anthropogenic climate change^{1–5}. The latest Intergovernmental Panel on Climatic Change (IPCC) consensus reports that global mean temperatures over the first two decades of the 21st century were 0.99 (0.84–1.10) °C higher than pre-Industrial levels (1850–1900 CE), and they are projected to exceed 1.5 °C above pre-Industrial levels by 2040⁶. In particular, the last two decades show a substantial increase in extreme summer temperatures worldwide^{7–12}. Understanding the spatial and temporal variations in the magnitude of these trends is critical because of the intrinsic coupling between climate extremes and ecological and socioeconomic systems.

In the summer of 2021, the Pacific Northwest region of the United States (US) and southwest Canada (hereafter the Pacific Northwest; PNW; 42–53 °N, 115–124 °W) experienced a prolonged, record-breaking heatwave starting in late June and continuing through early July. This extreme event was associated with an omega block atmospheric pattern that focused warmth over the PNW and caused daytime temperatures to reach 49.6 °C, increased wildfire activity¹³, elevated rates of heat-related deaths among PNW communities¹⁴, and ranks among one of the most anomalous, extreme heat events ever recorded globally during the observation period¹⁵. While the event lasted several weeks, the imprint of these extreme conditions is also apparent at longer timescales. In 2021, the PNW also experienced the highest mean summer (June–August; JJA) near-surface air temperatures on record over the observation period (1950–2021) (Fig. 1). Based on ERA5 reanalysis data, summer 2021 was approximately +3.6 °C warmer than the 1951–1980 average.

Extreme temperatures are some of the most significant climate impacts that human populations currently experience⁶, but communities around the world have different levels of vulnerability and resilience to the consequences of climate change^{16,17}. The timing and location of the PNW heatwave are particularly alarming, because none of the natural, socioeconomic, or infrastructural systems of the normally temperate PNW climate are currently adapted to prolonged extreme warmth. The inadequate regional infrastructure reflects a social perception that extreme warmth is not a substantial threat in this region of North America¹⁸. Prolonged heatwaves often go unrecognized as serious community health threats in temperate locations¹⁹, but when they do occur, indoor facilities are unable to provide heat relief for the most vulnerable populations. Compared to the US national average, significantly less homes in the PNW have primary air conditioning (AC)²⁰. While rates of AC use in British Columbia, Canada have nearly doubled in the last decade, as of 2020, still less than 40% of British Columbians have centralized household AC²¹, indicating a persistent vulnerability to warm temperature extremes. In addition to the immediate societal and health consequences, the effects of sustained temperature stress on forest ecosystems are visible across much of the PNW^{22,23}.

A growing body of literature, using limited observational data and modeling to characterize the historic nature of the 2021 PNW summer conditions, shows this event to be highly anomalous and of a magnitude with no comparable modern climatic analog^{24,25}. Rapid attribution suggests that the occurrence of this event would have been virtually impossible without anthropogenic climate change, but because the observed extreme temperatures were so far outside the range of historically observed temperatures (since ca. 1895), it is difficult to confidently quantify the rarity of the event²⁴. Augmenting the observational record with proxy data can

¹Tree-Ring Laboratory, Lamont-Doherty Earth Observatory of Columbia University, 61 Rte 9W, Palisades, New York 10964, USA. ²Department of Earth and Spatial Sciences, University of Idaho, 875 Perimeter Drive MS3021, Moscow, Idaho 83843, USA. ³School of Engineering, University of California–Merced, 5200 N. Lake Rd., Merced, California 95343, USA. ⁴Department of Geosciences, University of Arizona, 1064 Lowell Street, Tucson, Arizona 85721, USA. ⁵Department of Geoscience, University of Nevada, Las Vegas, 4505 Maryland Parkway, Las Vegas, Nevada 89119, USA. ⁶Department of Geography, Johannes Gutenberg University, Saarstraße 21, 55122 Mainz, Germany.

✉email: kheeter@ldeo.columbia.edu

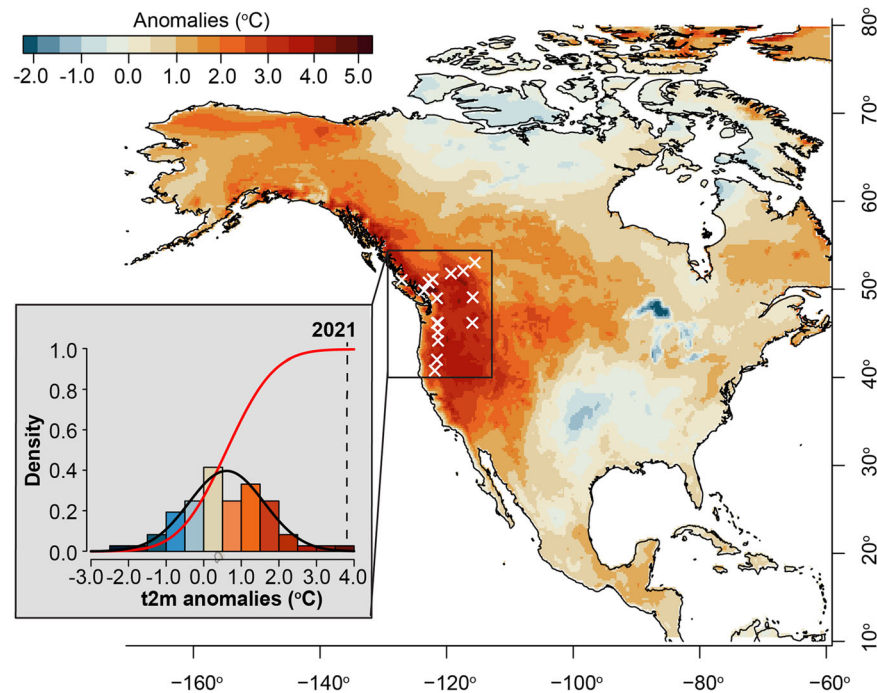


Fig. 1 The physical imprint and consequences of extreme summer heat across the Pacific Northwest in 2021. June–August (JJA) 2021 seasonally averaged temperature anomalies (t2m) over North America calculated from the 1951–1980 mean of ERA5 Reanalysis, with the Pacific Northwest region (PNW; 42–53 °N, 124–115 °W, dark blue box) highlighted. The year 2021 (dashed black line) is shown relative to the distribution (black line) and probability density (red line) curves of JJA t2m values over the period 1950–2021 for the PNW region. White exes indicate the locations of all tree-ring chronology predictors used in the subsequent JJA t2m reconstruction.

be an effective strategy for decreasing uncertainties related to longer-term climate variability, thereby leading to improved characterization and contextualization of recent warming trends and extreme events. Further, characterizing temporal variation in the rates of environmental change including extreme events is critical to better constrain future impacts and inform strategies for immediate climate change adaptation.

Across many regions of the Northern Hemisphere, the annual variability of tree growth, particularly metrics for wood density, strongly reflects the variation of summer season temperature^{26,27}. As such, tree-ring data can provide valuable temperature estimates prior to the influence of anthropogenic forcing, to which modern observations and future estimates can be compared. Here, we seek to provide improved estimates of long-term paleotemperature variability across the PNW, with which we can quantify how unusual summer temperatures in the PNW were in 2021 compared to not only the limited observational record, but the entire last millennium using a tree-ring-based reconstruction of mean summer near-surface temperatures (JJA t2m). This reconstruction is used to compare the record-breaking summer temperatures of 2021 and modern warming trends to conditions experienced during the last millennium, including during the Medieval Climate Anomaly (MCA; 950–1250 CE), a period characterized by shifts in large-scale Northern Hemisphere atmospheric circulation patterns and relatively warm temperature anomalies^{28,29}. Additionally, multi-model ensemble projections of Coupled Model Intercomparison Project Phase 6 (CMIP6) are used to compare and evaluate the likelihood of 2021-like heat through time.

RESULTS

PNW summer temperature estimates since 950 CE

The tree-ring latewood blue intensity and total-ring width records from 29 conifer collections across the PNW closely reflect near-

surface, average summer air temperatures (ERA5 t2m) over the region (Supplementary Fig. 1 and Supplementary Table 1). The strong relationship (Pearson's $r=0.87$, $p<0.01$) between the leading principal component of all tree-ring predictors and the ERA5 predictand data, allowed for the use of regression modeling to provide millennial-length historical temperature estimates, spanning the period 950–2021 CE (See Methods section, Supplementary Figs. 2, 3). The common calibration model explains 78% of the temperature variance over the period spanning 1950–2017 CE (Supplementary Fig. 2 and Supplementary Table 2). Indices of annual tree growth variability capture both year-to-year variability as well as longer-term temperature trends. As the number of tree-ring predictors decreases back through time, the explained variance of the reconstructions also decreases. The Medieval Era (prior to 1400 CE) is represented by only two tree-ring chronologies, but our reconstruction model still explains 45% of the temperature variance. The model is also highly skillful, with positive RE and CE statistics indicating a valid reconstruction back to 950 CE (Supplementary Table 2). Thus, while the earliest part of the reconstruction should be interpreted with additional caution due to increased uncertainty, our model statistics demonstrate that the reconstructed values provide robust insight into the temperature variability for the PNW region even during the MCA.

Summer average temperatures for 2021 are unprecedented since 950 CE (Fig. 2a). Probability density estimates based on normally-distributed ERA5 t2m data (1950–2021 CE) indicate that the 2021 summer average temperatures have a probability estimate of 0.004%, although substantial uncertainty exists for this estimate due to the short duration of instrumental data. Probability estimates based on reconstructed values (950–2021 CE) situate the 2021 summer average even further outside the normal range of historical variability documented across the PNW (Fig. 2b). The low-frequency (multi-decadal to centennial) summer temperature variability of the PNW reconstruction is highly correlated ($r=0.60$, $p<0.01$) with broader scale Northern

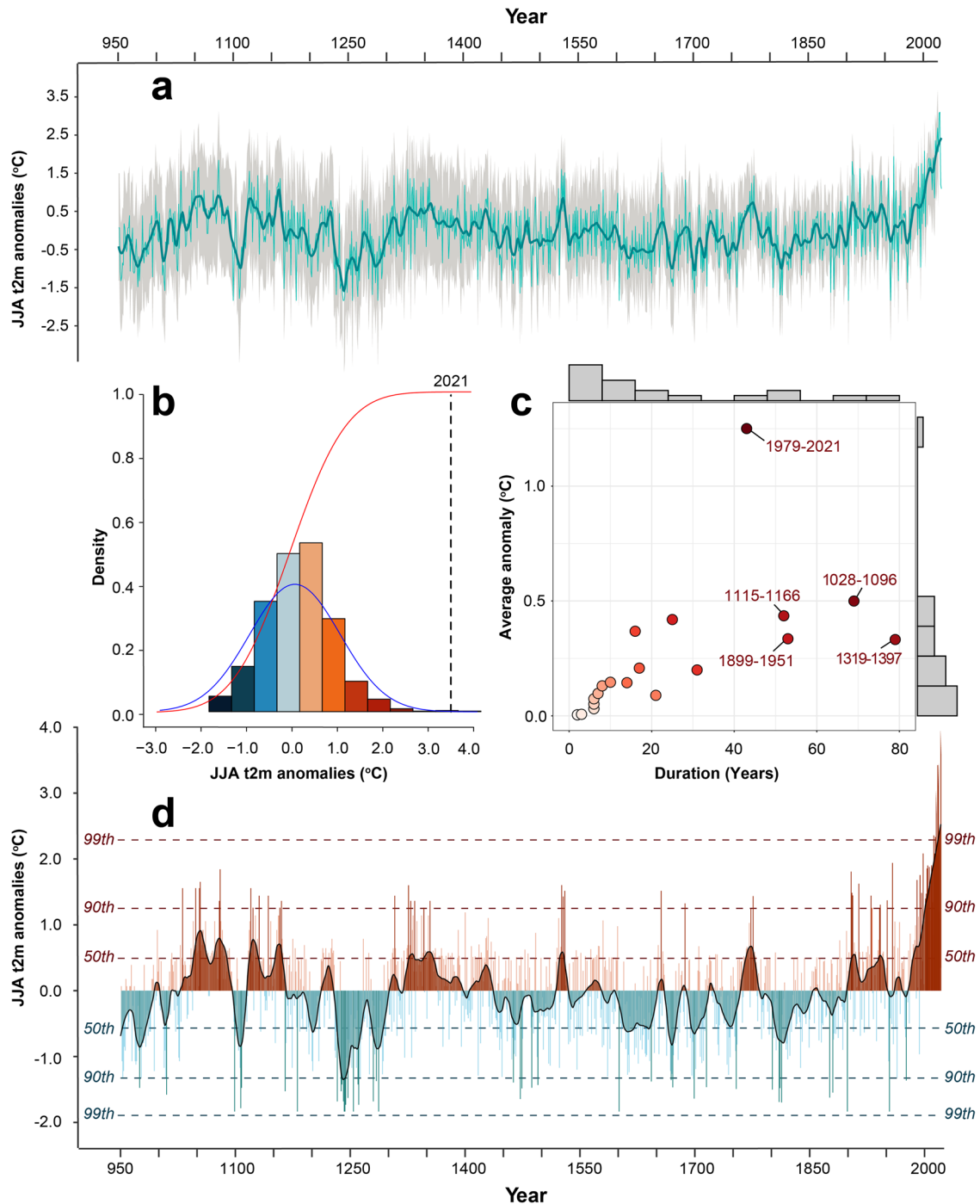


Fig. 2 Long-term estimates of summer temperature variability for the Pacific Northwest. Historical estimates of summertime mean temperatures (June–August t2m) over the Pacific Northwest from 950–2021 CE. **a** Annual reconstructed temperature anomalies (light teal line) relative to the 1951–1980 mean, with 10-year LOESS smoother (dark teal line) and associated error (gray line) of the model back through time. **b** Distribution of reconstructed temperature anomalies with the density distribution (blue line) and cumulative probability density function (red line) curves. **c** Bivariate characterization of multi-year warm events corresponding to time series in panel **d**. **d** Annual reconstructed temperature anomalies overlaid with 30-year LOESS smoothed time series of multi-year temperature departures, with the 50th, 90th, and 99th percentiles of all warm and cool departures denoted by horizontal dashed lines. Warm departures are colored red, and cold departures are colored blue. Warm and cool departures, which are at or exceed the 90th percentile, are denoted with dark red and blue bars, respectively.

Hemisphere paleotemperature estimates³⁰. However, our reconstruction offers a more detailed window into the climate history of the PNW and the influence of internal variability on the region's climate. The reconstruction documents numerous multi-decadal warm intervals over the last millennium. The record-breaking 2021 summer average was the culmination of an anomalous 43-

year warm period spanning the most recent decades (Fig. 2c, d). The period 1979–2021 CE ranks among one of the longest, continuous warm periods and has the highest average anomaly over the given period, averaging +1.27 °C above the 1951–1980 CE mean. While the 2021 value substantially increases the period's average anomaly, even without its inclusion, the period from

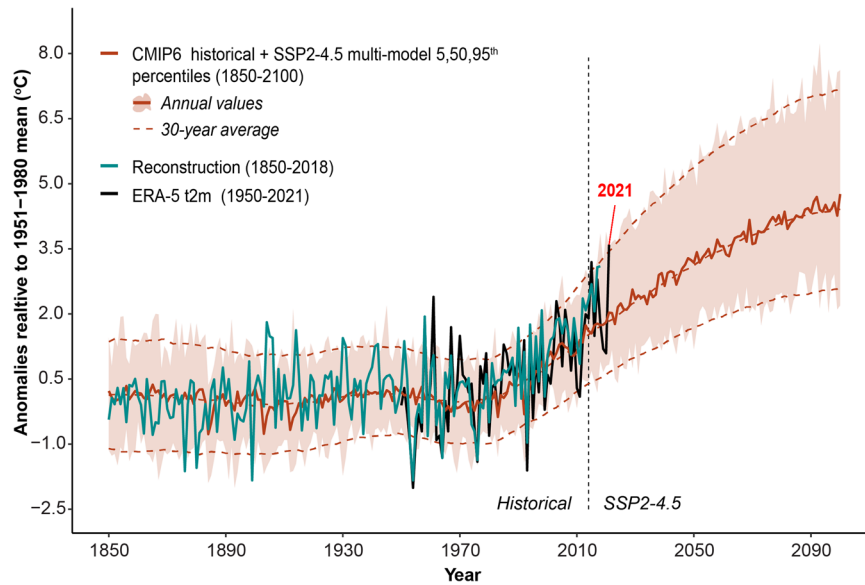


Fig. 3 Past, present, and future summer temperature trends for the Pacific Northwest. Comparison of reconstructed summer temperature anomalies (teal line), ERA5 t2m observational data (1950–2021; black line), and the annual (orange line and shading) and 30-year average (dashed orange lines) interquartile range (5th, 50th, and 95th percentiles) of regional CMIP6 historical runs (1850–2014 CE) and SSP2–4.5 multi-model ensemble estimates (2015–2100 CE), based on 40 members and over the period 1850–2100.

1979–2020 CE is still the warmest on record. The second-warmest period, in terms of average anomaly over the identified period, occurs during the MCA and spans 1028–1096 CE. Comparatively, the second-warmest 43-year warm period occurs from 1045–1087 CE, with an average anomaly of $+0.68^{\circ}\text{C}$. Even during the warmest interval of the MCA, mean of summer temperatures during this time are approximately 0.59°C cooler than those documented since 1979 CE. Decadal to multi-decadal warm periods during the mid-12th and 14th centuries are also features of the regional expression of the MCA. In addition to multi-decadal warm intervals, the reconstruction documents pronounced cooling from *ca.* 1240–1280, one of the longest cool intervals of the last millennium, prior to the Little Ice Age (*ca.* 1570–1900). Similar characterization of summer temperatures during the MCA are documented in the nearby Alberta Icefields reconstruction³¹ based on tree-ring maximum latewood density (Supplementary Fig. 4).

In terms of relative extremity, the 20th and 21st centuries are characterized by frequent average summer temperatures that rank within the top 90–99th percentiles of all positive departures documented over the last millennium (Fig. 2d). The reconstruction documents multiple historical warm periods, where at least one year during the respective period exceeds the 90th percentile, especially during the MCA (e.g., 1028–1096 CE and 1319–1397 CE). Compared to any of the positive temperature departures identified during the MCA, the magnitude of the 2021 departure is at least $+1.5^{\circ}$ warmer. Across the observational period (1950–present), the 2021 summer average is $+0.40$ warmer than the previous record summer average temperatures recorded in 2015. Comparing the long term, pre-Industrial period (950–1900 CE) to the full period (950–2021 CE), we document a shift to a positively skewed distribution of summer average temperatures (Supplementary Fig. 5). This positive shift documented for the PNW is akin to positive shifts in summer temperatures documented across North America as a direct result of anthropogenic CO_2 forcing³². Our reconstruction also reveals that the rate of warming over the most recent decades is unprecedented (Supplementary Fig. 6). The greatest rate of change over any given 20-year interval occurs from 1993–2012 CE, with a $+3.3^{\circ}\text{C}$ increase in summer temperatures over the period. Comparatively, the second most

rapidly warming 20-year interval occurs between 1107–1126 CE, marked by a $+2.9^{\circ}\text{C}$ change. Similarly, at 50-year intervals, the rate of summer warming beginning in the 1970s into the present is also the highest over the reconstructed period. Thus, while the PNW has experienced periods of anomalously warm summer temperature departures in the past, the modern warm extremes are of a substantially greater magnitude.

Future projections of PNW summertime temperatures

Our reconstruction provides a long-term, pre-Industrial (950–1850 CE) temperature baseline, prior to the effects of anthropogenic forcing, that can be used to evaluate future changes in climate. There is a strong agreement of trends in the ERA5 data, the reconstruction, and the CMIP6 historical runs over their respective shared periods (Fig. 3 and Supplementary Fig. 7). This is despite the effects of differences in relative forcing for each time series. The observed 2021 anomaly exceeds the 95th percentile of summer temperatures simulated by global circulation models participating in CMIP6 using SSP2–4.5 averaged over model years 2005–2035 ($+3.4^{\circ}\text{C}$). Similarly, the 2015 observed summer average anomaly ($+3.2^{\circ}\text{C}$) also exceeds the 95th percentile of CMIP6 SSP2–4.5 multi-model ensemble projections averaged over the period 1999–2029 ($+3.0^{\circ}\text{C}$). Kernel density estimates of modeled and observed summer temperature values over differing periods show an increase in both the mean and variance of temperature values above the long-term pre-Industrial (950–1850 CE) and current observational period (Fig. 4 and Supplementary Table 3). Compared to the long-term pre-Industrial, multi-model median CMIP6 SSP2–4.5 projections of average summer temperatures (2022–2100 CE) show an increase of more than $+3.0^{\circ}\text{C}$ (ranging from $+1.5$ to $+6.0^{\circ}\text{C}$).

The combination of both the historical runs (1950–2014 CE) and the ensemble medians of the CMIP6 SSP2–4.5 and SSP3–7.0 scenarios (2015–2100 CE) allow for further contextualization of the summer 2021 temperature anomaly in terms of future risk. SSP2–4.5 is considered a “middle of the road” scenario, while SSP3–7.0 represents a “medium-to-high-challenges” reference scenario, characterized by regional rivalry between countries³³. Here, the risk is defined as the percent chance of occurrence and is calculated from modeled temperature values relative to the

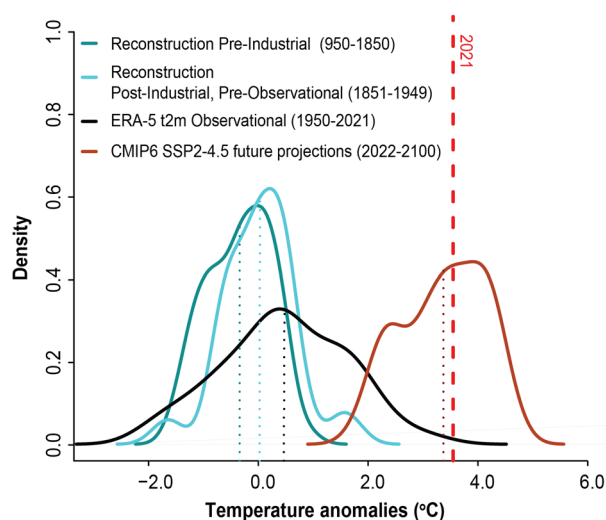


Fig. 4 The changing mean and distribution of summer temperature anomalies through time. Kernel density estimates of temperature anomaly values based on reconstruction values (dark and light teal lines), ERA5 values (black line), and CMIP6 SSP2-4.5 values (orange line) over time (950–2100 CE). For each Kernel density estimate, the dashed vertical lines indicate the mean for each respective density curve. The 2021 summer average anomaly for the PNW is denoted with a red dashed vertical line.

1951–1980 mean. Regionalized CMIP6 projections indicate that the likelihood of the PNW experiencing extreme summer temperatures analogous to 2021 ($+3.6^{\circ}\text{C}$) in any given year will reach 50–60% by 2050, depending on the SSP scenario (Fig. 5 and Supplementary Table 4). Even at the fifth percentile of multi-model ensembles, the risk of 2021-like summer heat reaches 50% by 2057 under the SSP3–7.0 scenario and by 2070 under the SSP2–4.5 scenario. Under the higher-end SSP3–7.0 scenario, the rate at which the risk of summers analogous to 2021 increase is particularly alarming; projections suggest that the contemporary risk of a $+3.6^{\circ}\text{C}$ summer anomaly is 5% (3–9% per year) (Supplementary Table 4), whereas by 2100, this risk increases to 94% (90–97% per year).

DISCUSSION

Examination of the 2-week-long 2021 PNW heatwave and its impact on 2021 summer average temperatures in the longer-term context illustrates another example in a growing body of evidence linking extreme weather events to anthropogenic climate change^{34–36}. A recent study using the observational record found the PNW 2021 summer to be a 1 in 1000-year event²⁴. In evaluating these extreme conditions from the paleo proxy perspective, which provides 1000+ years of historical temperature estimates, our results corroborate and augment previous modeled findings based solely on data from the observational record. These tree-ring-based temperature estimates provide new insights into the longer-term climate history of the PNW, where the MCA is characterized by several prolonged periods of above-average warmth and the presence of extreme, positive temperature departures. Substantial uncertainty with regards to the non-ubiquitous expression of the MCA still exists across the Northern Hemisphere²⁹, but the estimates from this study provide improvements for western North America. While conditions during the MCA are not equitable climate analogs to modern conditions across the PNW, identifying the severity and frequency of past extreme temperature departures as well as the range of natural internal variability is inherently valuable. Despite their

infrequency over the last *ca.* 1000 years, exceptionally hot temperature anomalies lead to the most severe losses for both natural and human communities^{12,17}. Previous work, using model-based experiments, identifies western North America as a locale where regional temperature variations appear to closely resemble global-scale temperature variation³⁷. As such, beyond the immediate benefit of the reconstruction providing geographically precise paleotemperature estimates spanning the last millennium for the PNW, the similarity between the PNW and Northern Hemisphere summer temperature reconstructions highlights the potential utility of this dataset for future assessments of large-scale temperature variability.

Compared to the last millennium, the 20th–21st centuries are marked by unprecedented warming and the occurrence of extreme summer temperatures across the PNW. Results from this study support previous work linking the significant increases in summer temperatures over the last several decades to anthropogenic climate change³⁸. Currently, summer averages across the PNW are warming at a rate comparable to the SSP2–4.5 scenario. At this rate, the previously unprecedented $+3.6^{\circ}\text{C}$ conditions documented across the PNW in summer 2021 will become a common occurrence in the absence of rapid mitigation efforts to curtail continued warming. Despite evidence that some CMIP6 models likely overestimate the degree of future warmth³⁹, an agreement between the reconstruction, the observational data, and the CMIP6 simulations over their shared periods (1850–2021 and 1950–2021, respectively) suggest that this issue may be less problematic for the PNW region^{40,41}.

Beyond anticipated mean warming, the PNW will likely experience an increased occurrence of extreme heat events in the future. Global projections suggest that the probability of occurrence of record-breaking temperatures is largely dependent on the overall warming, which is expected to continue to increase over the next few decades unless stabilized at or below the SSP1–2.6 scenarios⁴⁰. However, future projections of increasing occurrences of extreme seasons across the extratropical Northern Hemisphere are coupled with increased uncertainty. A major contributor to this increased uncertainty is the underestimation of the influence of internal variability in the current generation of coupled climate models⁴². As our reconstruction strongly captures the region-specific occurrence and magnitude of exceptional warm intervals through time, we emphasize the value of empirical tree-ring data, which allows us to better characterize internal variability and should lead to improved projections of extreme summer temperatures.

The unprecedented nature of 2021 summer temperatures across the PNW suggests that no region is impervious to the economic and biological impacts of increasing extreme summer temperatures. As in the PNW, communities across the world that have not been historically exposed to extreme heat are likely to experience greater negative impacts on increased morbidity and mortality because of the relative rarity of such events^{43,44}. Extreme heat events, amplified by rapid, multi-decadal warming, are catalysts of high-impact societal and ecosystem modification and will likely present substantial challenges to current and future climate change adaptation strategies. A recent analysis suggests that a renewed commitment to achieving the long-term target of the Paris Agreement⁴⁵ to limit warming to below 2.0°C and to pursuing efforts to limit warming to 1.5°C ⁴⁶ above pre-Industrial levels can be achieved if all obligations are implemented in full and on time⁴⁷. Concurrent with global emissions reduction efforts, long-term contextualization of historic climate events is important for identifying regional challenges to climate change adaptation strategies.

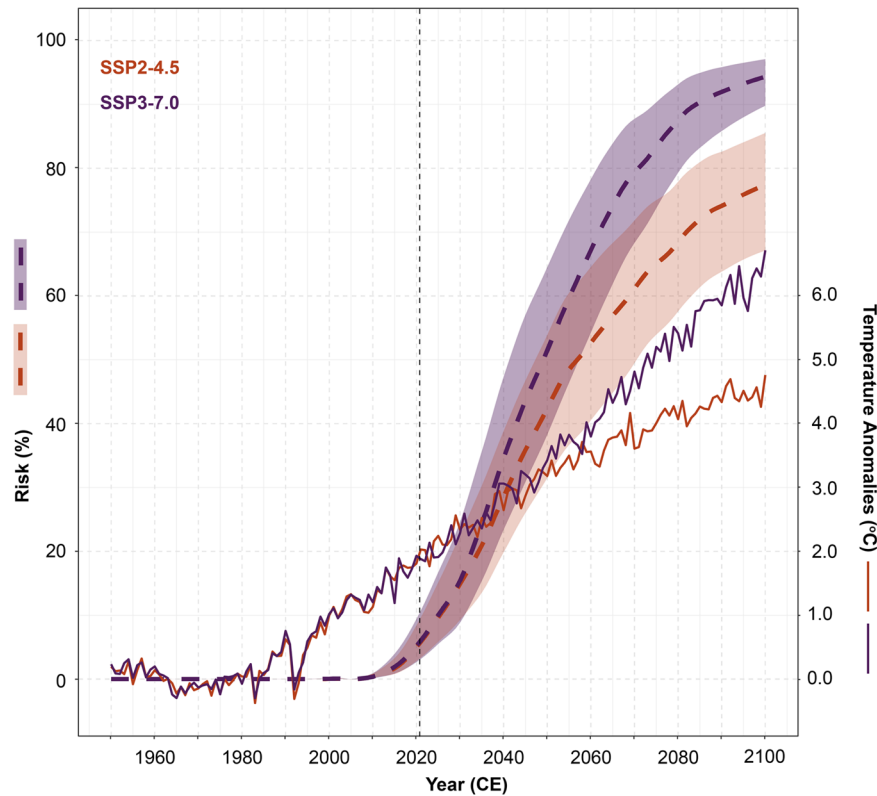


Fig. 5 Projected occurrence likelihood of summer temperatures analogous to 2021 (+3.6 °C) for the Pacific Northwest. Time evolution of summer temperature anomalies (right y-axis) over the Pacific Northwest region based on CMIP6 historical runs (1950–2014 CE), SSP2–4.5 (solid orange line), and SSP3–7.0 multi-model ensembles (solid purple line) (2015–2100 CE), with the time evolution of risk (left y-axis) associated with summer average anomalies greater or equal to the observed 2021 summer anomaly (+3.6 °C; dashed orange and purple lines). All risk calculations are derived from SSP2–4.5 and SSP3–7.0 multi-model ensembles and use anomalies relative to the 1951–1980 mean. Risk calculations are plotted using a 20-year LOESS smoother and include 95% confidence intervals. The year 2021 is marked with a dashed black line.

METHODS

Tree-ring data collection and preparation

We collected tree-ring samples from living trees growing in temperature-limited environments⁴⁸ across 17 sites in the Pacific Northwest region (42.0–53.0°N, 124.0–115.0°W). At each site, we collected increment cores from living trees (2 per tree). All tree-ring collections were collected and processed with the intent of collecting both total-ring width and latewood blue intensity (LWB) data. All samples were dried, mounted, and shaved with a core microtome⁴⁹ in order to achieve a flat planar surface. Samples were then polished with micron sandpaper. We removed any samples which exhibited discoloration due to fungal staining. As blue intensity measurements can be negatively affected by the presence of mobile wood compounds not confined to an individual annual ring, such as water and resins, we performed resin extraction prior to LWB measurement by passively soaking all cores in a 24 °C 99.5% ethanol bath for 96 h. With all resins removed, samples were re-shaved and fine-polished before data collection commenced.

Total-ring width and latewood blue intensity measurements were obtained for all samples using an Epson Expression XL 12000 commercial flatbed scanner in combination with the software Coorecorder⁵⁰. The absolute dating of all samples was statistically validated with the software COFECHA⁵¹. All tree-ring series were standardized (detrended) to remove age-related trends using the age-dependent spline (ADS) and variance stabilization on the power-transformed residuals in the SignalFree (SF) framework⁵². The SignalFree framework controls for trend distortion end effects in the curve fitting exercise and an age-dependent spline was

applied using an option that constrains its end behavior to be non-increasing. Consistent with findings from Yukon⁵³, the combination of SF and ADS, with this non-increasing constraint, greatly reduced the potential loss of a climate warming signal in the blue intensity chronologies used for the reconstruction.

Climate data

For the observational predictand, we used seasonally averaged (June–August) ERA5 Reanalysis mean temperature (t2m) data, averaged across the PNW for the period 1950–2021 CE. To compare the reconstruction with future projections, we compiled JJA seasonal CMIP6 SSP2–4.5 and SSP3–7.0 projections over the PNW region from all available ensemble members. We calculated the multi-model median as the 5th and 95th percentiles of CMIP6 SSP2–4.5 and SSP3–7.0 data based on 40 and 36 ensemble members, respectively.

Reconstruction model

We employed a nested principal components regression (PCR) model, which accounts for the change in the number of predictor chronologies through time⁵⁴. All detrended, site-level tree-ring chronologies were screened against local (within 0.50° of site location) temperature (mean, minimum, and maximum), precipitation, upper-level pressure, and drought index observation data prior to inclusion into the candidate predictor pool for the reconstruction. Only chronologies showing significant correlations with current-year summer temperatures were included in the predictor pool. We initially pre-whiten the predictor tree-ring chronologies and ERA5 data to provide a conservative estimate of

climate-predictor relationships that are not subject to inflation via auto-correlation.

Tree-ring chronologies were retained for modeling if they were positively and significantly ($p < 0.05$) correlated to the regionally-averaged target ERA5 data during the common period 1950–2017, using the Pearson, Robust Pearson, and Spearman correlation coefficients. In this study, 29 chronologies were retained for modeling. The original chronologies (non-pre-whitened) of significant predictors were then used in the PCR to develop the reconstructions. Following the Kaiser-Guttman rule, the first n eigenvectors with eigenvalues > 1 were retained for the PCR. The final subset of PCs was determined using the minimum Akaike information criterion, which includes a penalty term for increasing the number of predictors in the model⁵⁵.

We divided the instrumental period into an early (1950–1985) and late (1986–2018) period to validate, cross-validate, and test the reconstruction model for temporal stability. We performed model validation by calculating cross-calibration statistics for the full period (1950–2018) and verification statistics for the early period (1950–1985), as the earlier portions of the instrumental record often possess greater uncertainty than the latter part of the record⁵⁶. We used two goodness-of-fit tests, the reduction of error (RE) and coefficient of efficiency (CE), to validate the model^{48,54}. Positive RE values (ranges from $-\infty$ to $+1$) indicate that the calibration model is a more skillful predictor of the target data than the mean of the instrumental data during the calibration period. The validation statistics produced were the calibration and verification period coefficient of determination (CRSQ and VRSQ), and the validation period reduction of error and coefficient of efficiency (VRE and VCE). We quantified model uncertainty with maximum entropy bootstrapping (MEBoot)^{57,58} based on 300 reconstruction replicates. As nests dropped out through time, we employed a variance stabilization technique where we re-scaled each nest to the preceding, more replicated nest over the period of common overlap. Final reconstruction values were then bias-corrected to the ERA5 data⁵⁹. Because tree-ring predictors end in 2018, ERA5 data were added to the end of the reconstruction to account for 2019–2021.

Statistical analysis

Prior to subsequent analysis, all reconstructed temperature values were transformed into anomalies, relative to the 1951–1980 climate normal. In order to compare the unusual nature of the summer 2021 average temperature value in the context of the last millennium (950–2021 CE) versus the observational period (1950–2021), we calculated probability density functions based on the Gaussian distribution of all ERA5 and reconstructed temperature values. In order to identify and characterize multi-year warm and cool periods, we applied a 30-year locally weighted regression (LOESS) smoother on the reconstruction time series. Placing an additional emphasis on historical warm periods, we compared all identified warmer-than-average periods using a bivariate analysis, where we quantified the duration and the average anomaly over the identified period. Using the non-smoothed reconstruction anomaly values, extreme departures were determined by calculating the 50th, 90th, and 99th percentiles of all warm and cool anomalies over the entire reconstructed period, with values exceeding the 90th percentile (either warm or cool) being considered extreme years. Separately, we also assessed multi-decadal trends by calculating an index of percent change over time using backward-moving 20 and 50-year windows on reconstruction values.

The temperature reconstruction was compared to an independent Northern Hemispheric ensemble MJJA mean temperature reconstruction based on a data assimilation approach³⁰, as well as the Alberta Icefields MJJA, mean temperature reconstruction³¹. Reconstructions were transformed to z-scores, calculated using

their respective 1951–1980 mean and standard deviation values. We evaluated the relationship between the low-frequency trends of both reconstructions using a rolling 51-year Pearson correlation with the RolWinCor package in R⁶⁰.

Annual observed (ERA5) summer average anomalies, particularly 2021, were initially compared to average values for the 5th, 50th, and 95th percentiles of CMIP6 historical runs and SSP2–4.5 projections, calculated over 30-year moving windows. To evaluate changes in the distribution and mean of temperature estimates through time, we provided kernel density estimates of anomaly time series from the reconstruction, the ERA5 reanalysis data on which the reconstruction was based, and the multi-model median of annual CMIP6 SSP2–4.5 projections, calculated from the 1951–1980 mean. The full period mean was calculated for each time series and plotted with the corresponding kernel density estimate. Warming trends in the ERA5, reconstructed, and CMIP6 historical runs t2m anomaly time series were quantified as the change in $^{\circ}\text{C}$ per year over the shared period 1950–2014. To evaluate the likelihood of 2021 summer conditions in the future, we calculated future risk using multi-model ensemble data from CMIP6 SSP2–4.5 and SSP3–7.0 (all forcings) over the period 1950–2100 CE. We define “risk” as the probability of occurrence. The probability of occurrence of summer temperatures reaching 3.6°C was calculated using continuous probability density functions, calculated from the distribution of data values from all member models for each given year and assuming the Gaussian distribution of data values. The probabilities of the 5th and 95th percentiles were also calculated.

DATA AVAILABILITY

All data detailed in this manuscript will be made available upon request by the authors. All ERA5 data used in this study are available through the World Meteorological Organization- Koninklijk Nederlands Meteorologisch Instituut Climate Explorer (<https://climexp.knmi.nl/>). All historical and CMIP6 projection data are available at (<https://cds.climate.copernicus.eu/cdsapp#/dataset/projections-cmip6>). The reconstruction and tree-ring data can be found through the NOAA Paleoclimatology data bank.

Received: 18 August 2022; Accepted: 8 February 2023;

Published online: 17 February 2023

REFERENCES

- Eyring, V. et al. in *Climate Change 2021: The Physical Science Basis. Contribution of Working Group I to the Sixth Assessment Report of the Intergovernmental Panel on Climate Change* (eds Masson-Delmotte, V. et al.) Ch. 3 (Cambridge Univ. Press, 2021).
- Gulev, S. K. et al. in *Climate Change 2021: The Physical Science Basis. Contribution of Working Group I to the Sixth Assessment Report of the Intergovernmental Panel on Climate Change* (eds Masson-Delmotte, V. et al.) Ch. 2 (Cambridge Univ. Press, 2021).
- Perkins, S., Alexander, L. & Nairn, J. Increasing frequency, intensity and duration of observed global heatwaves and warm spells. *Geophys. Res. Lett.* **39**, L20714 (2012).
- AghaKouchak, A. et al. Climate extremes and compound hazards in a warming world. *Annu. Rev. Earth Planet. Sci.* **48**, 519–548 (2020).
- van der Wiel, K. & Bintanja, R. Contribution of climatic changes in mean and variability to monthly temperature and precipitation extremes. *Commun. Earth Environ.* **2**, 1–11 (2021).
- Masson-Delmotte, V. et al. *Contribution of Working Group I to the Sixth Assessment Report of the Intergovernmental Panel on Climate Change* (Cambridge Univ. Press, 2021).
- Sun, Y. et al. Rapid increase in the risk of extreme summer heat in Eastern China. *Nat. Clim. Change* **4**, 1082–1085 (2014).
- Christidis, N., Jones, G. S. & Stott, P. A. Dramatically increasing chance of extremely hot summers since the 2003 European heatwave. *Nat. Clim. Change* **5**, 46–50 (2015).
- Coumou, D. & Rahmstorf, S. A decade of weather extremes. *Nat. Clim. Change* **2**, 491–496 (2012).

10. Seneviratne, S. I., Donat, M. G., Mueller, B. & Alexander, L. V. No pause in the increase of hot temperature extremes. *Nat. Clim. Change* **4**, 161–163 (2014).
11. Climantartide. Antarctic meteo-climatological observatory real time data: temperature [oC]. <https://www.climantartide.it/realtime/index.php?lang=en> (2022).
12. India Meteorological Department. India meteorological department observations —maximum temperatures. (2022).
13. Overland, J. E. Causes of the record-breaking Pacific northwest heat-wave, late June 2021. *Atmosphere* **12**, 1434 (2021).
14. Henderson, S. B., McLean, K. E., Lee, M. J. & Kosatsky, T. Analysis of community deaths during the catastrophic 2021 heat dome: early evidence to inform the public health response during subsequent events in greater Vancouver, Canada. *Environ. Epidemiol.* **6**, e189 (2022).
15. Thompson, V. et al. The 2021 western North America heat wave among the most extreme events ever recorded globally. *Sci. Adv.* **8**, eabm6860 (2022).
16. Hsiang, S. et al. Estimating economic damage from climate change in the United States. *Science* **356**, 1362–1369 (2017).
17. Portner, H. O. et al. *Climate Change 2022: Impacts, Adaptation and Vulnerability* (Cambridge Univ. Press, 2022).
18. Maas, A., Wardrop, C., Roesch-McNally, G. & Abatzoglou, J. The (mis) alignment of farmer experience and perceptions of climate change in the US inland Pacific Northwest. *Clim. Change* **162**, 1011–1029 (2020).
19. Henderson, S. B., McLean, K. E., Kosatsky, T. Extreme heat events are public health emergencies. *BC Med. J.* **63**, 366–367 (2021).
20. United States Census Bureau. American housing survey: top 15 metropolitan areas - heating, air conditioning, and appliances - all occupied units. (2019).
21. BC Hydro. BC hydro residential end use survey. (2020).
22. Bumbaco, K. A., Dello, K. D. & Bond, N. A. History of Pacific Northwest heat waves: synoptic pattern and trends. *J. Appl. Meteorol. Climatol.* **52**, 1618–1631 (2013).
23. Halofsky, J. E., Peterson, D. L. & Harvey, B. J. Changing wildfire, changing forests: the effects of climate change on fire regimes and vegetation in the Pacific Northwest, USA. *Fire Ecol.* **16**, 1–26 (2020).
24. Philip, S. Y. et al. Rapid attribution analysis of the extraordinary heatwave on the Pacific Coast of the US and Canada June 2021. *Earth Syst. Dyn. Discuss.* **13**, 1689–1713 (2021).
25. McKinnon, K. A. & Simpson, I. R. How unexpected was the 2021 Pacific Northwest heatwave? *Geophys. Res. Lett.* **49**, e2022GL100380 (2022).
26. Briffa, K. R., Jones, P. D., Schweingruber, F. H. & Osborn, T. J. Influence of volcanic eruptions on northern hemisphere summer temperature over the past 600 years. *Nature* **393**, 450–455 (1998).
27. Wilson, R. et al. Last millennium Northern Hemisphere summer temperatures from tree rings: Part I: the long-term context. *Quat. Sci. Rev.* **134**, 1–18 (2016).
28. Graham, N. E., Ammann, C. M., Fleitmann, D., Cobb, K. M. & Luterbacher, J. Support for global climate reorganization during the “Medieval Climate Anomaly”. *Clim. Dyn.* **37**, 1217–1245 (2011).
29. Mann, M. E. et al. Global signatures and dynamical origins of the Little Ice Age and Medieval Climate Anomaly. *Science* **326**, 1256–1260 (2009).
30. King, J. M. et al. A data assimilation approach to last millennium temperature field reconstruction using a limited high-sensitivity proxy network. *J. Clim.* **34**, 7091–7111 (2021).
31. Luckman, B. & Wilson, R. Summer temperatures in the Canadian Rockies during the last millennium: a revised record. *Clim. Dyn.* **24**, 131–144 (2005).
32. McKinnon, K. A., Rhines, A., Tingley, M. P. & Huybers, P. The changing shape of Northern Hemisphere summer temperature distributions. *J. Geophys. Res. Atmos.* **121**, 8849–8868 (2016).
33. O'Neill, B. C. et al. The scenario model intercomparison project (ScenarioMIP) for CMIP6. Geoscientific model. *Development* **9**, 3461–3482 (2016).
34. Stott, P. A. et al. Attribution of extreme weather and climate-related events. *Wiley Interdiscip. Rev. Clim. Change* **7**, 23–41 (2016).
35. Fischer, E. M. & Knutti, R. Anthropogenic contribution to global occurrence of heavy-precipitation and high-temperature extremes. *Nat. Clim. Change* **5**, 560–564 (2015).
36. Bartusek, S., Kornhuber, K. & Ting, M. 2021 North American heatwave amplified by climate change-driven nonlinear interactions. *Nat. Clim. Change* **12**, 1143–1150 (2022).
37. Jones, P. D., Bradley, R. S. & Jouzel, J. (eds) *Climatic Variations and Forcing Mechanisms of the Last 2000 Years* Vol. 41 (Springer Science & Business Media, 2013).
38. Abatzoglou, J. T., Rupp, D. E. & Mote, P. W. Seasonal climate variability and change in the Pacific Northwest of the United States. *J. Clim.* **27**, 2125–2142 (2014).
39. Hausfather, Z., Marvel, K., Schmidt, G. A., Nielsen-Gammon, J. W. & Zelinka, M. Climate simulations: recognize the ‘hot model’ problem. *Nature* **605**, 26–29 (2022).
40. Tokarska, K. B. et al. Past warming trend constrains future warming in CMIP6 models. *Sci. Adv.* **6**, eaaz9549 (2020).
41. Ribes, A., Qasmi, S. & Gillett, N. P. Making climate projections conditional on historical observations. *Sci. Adv.* **7**, eabc0671 (2021).
42. O'Reilly, C. H. et al. Projections of northern hemisphere extratropical climate underestimate internal variability and associated uncertainty. *Commun. Earth Environ.* **2**, 1–9 (2021).
43. Fischer, E. M., Sippel, S. & Knutti, R. Increasing probability of record-shattering climate extremes. *Nat. Clim. Change* **11**, 689–695 (2021).
44. Meehl, G. A. & Tebaldi, C. More intense, more frequent, and longer lasting heat waves in the 21st century. *Science* **305**, 994–997 (2004).
45. UNFCCC. Paris Agreement. I: proposal by the President (Draft Decision) (United Nations Office, 2015).
46. Lennan, M. & Morgera, E. The Glasgow Climate Conference (COP26). *Int. J. Mar. Coast. Law* **37**, 137–151 (2022).
47. Meinshausen, M. et al. Realization of Paris Agreement pledges may limit warming just below 2 °C. *Nature* **604**, 304–309 (2022).
48. Fritts, H. *Tree Rings and Climate* (Elsevier, 2012).
49. Gärtner, H. & Nievergelt, D. The core-microtome: a new tool for surface preparation on cores and time series analysis of varying cell parameters. *Dendrochronologia* **28**, 85–92 (2010).
50. Larsson, L. CooRecorder and C dendro programs of the CooRecorder/C-dendro package version 7.7 (2014).
51. Holmes, R. L. Computer-assisted quality control in tree-ring dating and measurement. *Tree-Ring Bull.* **43**, 69–75 (1983).
52. Melvin, T. M., Briffa, K. R., Nicolussi, K. & Grabner, M. Time-varying- response smoothing. *Dendrochronologia* **25**, 65–69 (2007).
53. Wilson, R. et al. Improved dendroclimatic calibration using blue intensity in the southern Yukon. *Holocene* **29**, 1817–1830 (2019).
54. Cook, E. R., Meko, D. M., Stahle, D. W. & Cleaveland, M. K. Drought reconstructions for the continental United States. *J. Clim.* **12**, 1145–1162 (1999).
55. Akaike, H. A new look at the statistical model identification. *IEEE Trans. Autom. Control* **19**, 716–723 (1974).
56. Cook, E. R. et al. Tree-ring reconstructed summer temperature anomalies for temperate East Asia since 800 CE. *Clim. Dyn.* **41**, 2957–2972 (2013).
57. Vinod, H. D. et al. Maximum entropy bootstrap for time series: the meboot r package. *J. Stat. Softw.* **29**, 1–19 (2009).
58. Cook, E. R. et al. Five centuries of Upper Indus River flow from tree rings. *J. Hydrol.* **486**, 365–375 (2013).
59. Robeson, S. M., Maxwell, J. T. & Ficklin, D. L. Bias correction of paleoclimatic reconstructions: a new look at 1,200+ years of Upper Colorado River flow. *Geophys. Res. Lett.* **47**, 2019–086689 (2020).
60. Polanco-Martinez, J. M. Rolwinmulcor: an r package for estimating rolling window multiple correlation in ecological time series. *Ecol. Inform.* **60**, 101163 (2020).

ACKNOWLEDGEMENTS

This research was supported by National Science Foundation under AGS-2002524, AGS-1803995, and BCS-1759629. We would like to thank all field assistants who helped with sample collection as well as the International Blue Intensity Network Development (I-BIND) working group.

AUTHOR CONTRIBUTIONS

K.J.H.: Project conceptualization, acquisition of data and materials, data analysis, manuscript writing, manuscript editing, and final approval of the completed version. G.L.H.: Project conceptualization, acquisition of data and materials, manuscript editing, and final approval of the completed version. J.T.A.: Project conceptualization, acquisition of data and materials, manuscript editing, and final approval of the completed version. K.J.A.: acquisition of data and materials, data analysis, manuscript editing, and final approval of the completed version. E.R.C., B.L.C., L.A.D., and I.K.H.: acquisition of data and materials, manuscript editing, and final approval of the completed version.

COMPETING INTERESTS

The authors declare no competing interests.

ADDITIONAL INFORMATION

Supplementary information The online version contains supplementary material available at <https://doi.org/10.1038/s41612-023-00340-3>.

Correspondence and requests for materials should be addressed to Karen J. Heeter.

Reprints and permission information is available at <http://www.nature.com/reprints>

Publisher's note Springer Nature remains neutral with regard to jurisdictional claims in published maps and institutional affiliations.



Open Access This article is licensed under a Creative Commons Attribution 4.0 International License, which permits use, sharing, adaptation, distribution and reproduction in any medium or format, as long as you give appropriate credit to the original author(s) and the source, provide a link to the Creative Commons license, and indicate if changes were made. The images or other third party material in this article are included in the article's Creative Commons license, unless indicated otherwise in a credit line to the material. If material is not included in the article's Creative Commons license and your intended use is not permitted by statutory regulation or exceeds the permitted use, you will need to obtain permission directly from the copyright holder. To view a copy of this license, visit <http://creativecommons.org/licenses/by/4.0/>.

© The Author(s) 2023